

Miniaturized Laser Diode Driver and Microwave Source for
Transportable Quantum Sensors

Peer-reviewed author version

Li, Zheyi; Kim, SinNyoung; TAVAKOLI DINANI, Reza; Zhang , Yijing; Eryilmaz, Ilker; Berti, Laurent & NESLADEK, Milos (2024) Miniaturized Laser Diode Driver and Microwave Source for Transportable Quantum Sensors. In: 2024 IEEE 20Th Asia Pacific Conference on circuits ans systems, Apccas 2024, IEEE, p. 344 -348.

DOI: 10.1109/APCCAS62602.2024.10808645

Handle: <http://hdl.handle.net/1942/45566>

Miniaturized Laser Diode Driver and Microwave Source for Transportable Quantum Sensors

Zheyi Li*, SinNyoung Kim*, Reza Tavakoli Dinani†, Yijing Zhang*, Ilker Eryilmaz*, Laurent Berti* and Milos Nesladek†

* Department of ICLINK, imec, Leuven, Belgium

† Hasselt University, Martelarenlaan 42, B-3500 Hasselt, Belgium
IMOMEC Division, IMEC, Kapeldreef 75, B-3001 Leuven, Belgium.

Abstract— The nitrogen-Vacancy (NV) defect center is a promising tool to build magnetic sensors for space applications. This paper presents an ASIC solution of two key blocks in such a sensor: a laser diode driver (LDD) and a microwave (MW) source by a voltage-controlled oscillator (VCO) structure. This application requires that LDD has a wide driving current tuning range and enables a stable LD power insensitive to temperature changes. It also requires that the VCO can generate the MW frequency with three tunable parameters (carrier, modulation and deviation frequency) by a stand-alone design. Designed in a 65-nm technology, the LDD achieves a current tunable from 88.2 mA to 311.3 mA and shows only 0.17 mW deviation at 80 mW working power across a temperature range of 60 °C, and the VCO could reach a carrier frequency range of 2.37 GHz to 3.25 GHz with a modulation frequency of up to 5 MHz and a deviation frequency of up to 6 MHz, according to the post-layout simulation. The two blocks now only occupy an area of 0.79 mm² and a power consumption of 4.8 mW, which paves the way for a compact, transportable NV magnetic sensor suitable for future space exploration.

Keywords—Quantum magnetic sensor, Nitrogen-Vacancy defect center, laser diode driver, inductance capacitance voltage-controlled oscillator (LC-VCO)

I. INTRODUCTION

Over the last 15 years, defect centers in solid-state materials have attracted extensive attention in applications of quantum sensing, computing and communication [1-2]. In particular, the Nitrogen-Vacancy (NV) defect centers in diamonds have been proven as a promising platform to conduct sensitive magnetic measurements and can be made into the scalar, vector, DC or AC magnetometers [3-6]. Recently, this magnetic sensor has also been considered as an attractive candidate in space applications for various purposes, e.g., the earth observatory, ionospheric measurement activities and solar system exploration [7]. In the space application, miniaturization, compactness and low power consumption are the key features due to the limited area and power resources in the space. However, the current available NV magnetic sensors are only built with bulky and expensive optical and electronic equipment, making the system not portable or easily accessible. Therefore, there comes a great demand to develop a compact, easy-to-use and transportable magnetic sensor suitable for space exploration. In this work, two of the main sub-systems in the entire quantum sensor system, i.e., the laser diode driver (LDD) and the microwave (MW) source, are designed by ASIC, which is one of the first miniaturization attempts for this particular sensor type.

This paper is organized as follows: the principle of NV magnetic sensor is first explained in Section II. Section III

This research was funded by the European Union’s Horizon Europe research and innovation program under grant agreement No. 101080136 (AMADEUS).

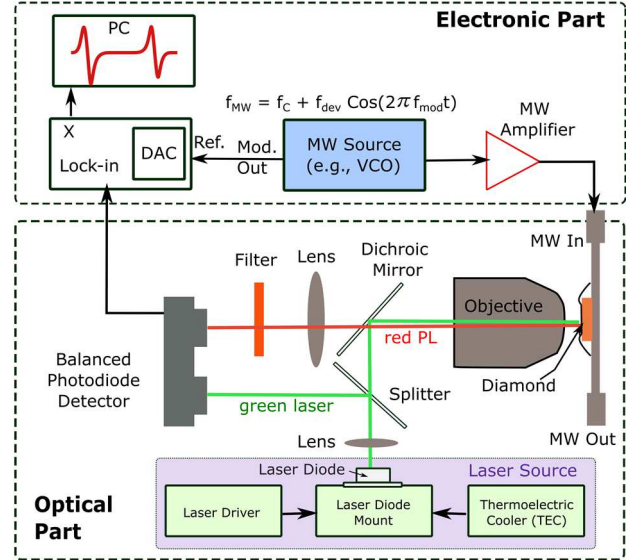


Fig. 1: Overview of a setup used to measure magnetic field using NV defects in diamond.

then demonstrates the design details of the customized LDD and MW source. Section IV presents the post-layout simulation results, and conclusions are drawn in Section VI.

II. TRANSPORTABLE QUANTUM SENSING SYSTEM OVERVIEW

A typical magnetic sensing setup based on NV defect center in diamond, as shown in Fig. 1, contains two main parts: the optical part and the electronic part. The optical part mainly includes the laser source, photodiode detector, diamond, and other optical components (e.g., lens, splitter). The electronic part includes the MW amplifier, MW source and other data acquisition and control units.

The laser source emits a visible green laser at a wavelength of 520-532 nm, which is used to prepare the electron spins of negatively charged NV centers, i.e., NV⁻, in their ground states [8]. Once the diamond is illuminated by the green light, it starts emitting red photoluminescence (PL), which can be monitored by the photodiode.

The MW source drives electron spin population between ground states. To achieve this, the frequency of the MW field f_{MW} must be resonant with the frequency splitting between the ground states. In the absence of any magnetic field, this splitting frequency is called zero-field-splitting $D = 2.87$ GHz and in the presence of a static magnetic field is $D \pm B_0 \gamma_e / 2\pi$, where γ_e is the electron gyromagnetic ratio and B_0 is the projection of a static magnetic field along the sensing axis of the diamond lattice. Once the resonance condition is met, the ground state population changes and appears as variations in the PL signal.

To measure the magnetic field of interest B_{sens} from the environment (e.g., earth magnetic field or ionospheric activities), the f_{MW} needs to be swept around the resonance frequency, and the PL signal, which looks like two Lorentzian profiles with separate centers separated by $D \pm (B_0 + B_{\text{sens}})\gamma_e/2\pi$, will be monitored. However, in this way, the PL signal could suffer from the high susceptibility to the low frequency noise. A typical method to overcome this issue is the frequency-modulated technique [9], in which the frequency of MW changes periodically as

$$f_{\text{MW}} = f_c + f_{\text{DEV}}\sin(2\pi f_{\text{MOD}}t) \quad (1)$$

where f_c , f_{MOD} and f_{DEV} are carrier, modulation and deviation frequencies, respectively. As a result, the PL signal will be modulated at f_{MOD} and its amplitude can be detected using the phase sensitive detector (PSD). By sweeping the f_{MW} , the PSD output performs a dispersive pattern. The interest magnetic field B_{sens} can then be obtained from monitoring this PSD output by tuning f_{MW} within a linear regime. More details about the physics and principle of the NV-based sensor can be found in [1].

The application puts forward design requirements for the laser diode driver and MW source in this system. In this work, a commercial green laser diode (Osram PLT5 520B) [10] is selected to produce the laser. A laser driver is then needed to provide a wide driving current range and control the diode power to work at a stable power regardless of the temperature change. The currently available LDDs are either bulky equipment or discrete-component designs. In this paper, a compact ASIC solution is proposed.

Regarding the MW source, a voltage control oscillator (VCO) has been proven to be a good candidate for generating the frequency-modulated MW signal f_{MW} . However, the available commercial VCOs can only cover part of the MW frequency range since they cannot produce the 3 frequencies (f_c , f_{MOD} , f_{DEV}) in (1) alone. Therefore, a dedicated stand-alone VCO is proposed to fulfill this target in this paper. The f_c is decided from 2.37 GHz to 3.25 GHz to ensure about ± 500 MHz frequency offset from the zero-splitting frequency of $D=2.87$ GHz. The f_{MOD} is supposed to be large enough to have f_{MW} away from low-frequency noise sources. The previous experiments show the f_{MOD} can reach an upper limit of 100 kHz, considering different experimental conditions and supplementary materials. As for the f_{DEV} , it depends on the linewidth Γ of NV centers, which is typically in a range of 1 to 2 MHz.

III. CIRCUIT DESIGN

A. Laser Diode Driver

The principle of the LDD is demonstrated in Fig. 2 (top left). The utilized laser diode (Osram PLT5 520B) contains an emission diode and a photonic diode [10]. The emission diode is responsible for producing the green laser. However, its power P_F is sensitive to the driving current I_F and the ambient temperature T . The photonic diode is a monitor element that generates a current I_M proportional to the P_F . From the application request, the emission diode should work at a power that is always stable in the presence of temperature change and also programmable in a needed range.

A dedicated diode driver is therefore designed. As shown in Fig. 2 (top left), the diode driver uses a transconductance (G_m) stage to control the driving current I_F and the power P_F . In order to tackle the temperature effect, the I_M current of the

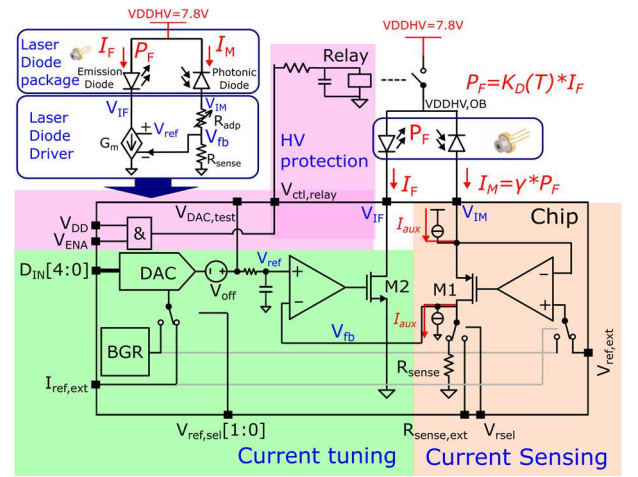


Fig. 2. Laser diode driver principle (top left) and detailed block diagram (bottom).

photonic diode is sensed by a resistor R_{sense} and fed back negatively to the G_m stage. The P_F can then be derived as

$$P_F = \frac{V_{\text{ref}} \cdot G_m \cdot K_D(T)}{1 + R_{\text{sense}} \cdot G_m \cdot \gamma \cdot K_D(T)} \approx \frac{1}{R_{\text{sense}} \cdot \gamma} \cdot V_{\text{ref}} \quad (2)$$

where $K_D(T)$ models the temperature-sensitive relation between the P_F and I_F , and γ is the monitor ratio between I_M and P_F . It indicates that if $R_{\text{sense}} \cdot G_m \cdot \gamma \cdot K_D(T) \gg 1$, which is the case in this design, the temperature coefficient of the P_F becomes negligible. Moreover, this equation can be further elaborated as

$$P_F \approx \frac{1}{R_{\text{sense}} \cdot \gamma} \cdot V_{\text{ref}} = \frac{\sum_{i=1}^4 D_{\text{IN}}[i] \cdot I_{\text{DAC}} \cdot R_{\text{DAC}} \cdot T_{\text{CR}} + V_{\text{off}}}{R_{\text{sense}} \cdot T_{\text{CR}} \cdot \gamma} \approx \frac{\sum_{i=1}^4 D_{\text{IN}}[i] \cdot I_{\text{DAC}} \cdot R_{\text{DAC}}}{R_{\text{sense}} \cdot \gamma} \quad (3)$$

In (3), V_{ref} is composed by the addition of a current steering DAC output and an offset voltage, where R_{DAC} is the DAC resistor element, and T_{CR} is the temperature coefficient of resistance, which applies to both R_{DAC} and R_{sense} . Because V_{off} is a small value (< 5 LSBs), which is negligible compared to the DAC output, the T_{CR} from the R_{DAC} and R_{sense} are canceled. As a result, P_F is not relevant to temperature.

In the implementation of the LDD, there are more requirements raised by the diode, the technology and the use case. Firstly, the photonic diode requires a fixed 5V reverse voltage. Secondly, all the node-to-node voltages cannot exceed 3.63V to avoid breakdown at the 65nm technology. Thirdly, the previous two guidelines should be fulfilled under the entire use scenario, including the power-up stage and all the programming conditions.

The detailed block diagram of the LDD is presented in Fig. 2 (bottom) and can be divided into three parts: current tuning, current sensing and high voltage protection.

At the top of the current sensing part, a PMOS transistor (M1) driven by an amplifier, which becomes the current sensing loop, is employed to bias V_{IM} at 2.8 V and maintain the 5 V voltage drop across the photonic diode. However, when I_F is low at the low P_F scenario, the sensing loop becomes unstable due to the low current flows to the biased M1 transistor. An auxiliary current source and drain pair is added to provide a minimum current I_{aux} for the I_M path and stabilize the loop. Under this loop, there is the R_{sense} to create the feedback voltage V_{fb} from the monitor current I_M .

In the current tuning part, an NMOS transistor (M2) driven by an operational amplifier forms the G_m stage. The amplifier's positive node is provided by a 5-bit current-steering DAC output plus the offset voltage. Its negative node comes from the current sensing part and forms a current tuning loop. In the case that I_F approaches a zero, which could shut down the NMOS transistor and force $V_{IF}=V_{DDHV}$, this offset voltage is inserted. The V_{off} is selected such as the V_{IF} is kept at a safe value and the I_F is kept less than the threshold current of the emission diode in this extreme case. Moreover, since the current tuning loop is based on the output of the current sensing loop, its bandwidth should be designed to be larger to ensure sufficiently fast feedback.

In the start-up phase, it is critical that the LDD is powered up (by V_{DD}) prior to the laser diode (by V_{DDHV}). Otherwise, the 7.8V voltage could easily pass to the LDD and break the transistors. To avoid this, a high-voltage protection scheme is implemented. Only when the LDD supply V_{DD} and the enable signal V_{ENA} are activated, the off-chip relay switch will turn on the diode, after a fixed delay introduced by a low-pass filter.

B. High tuning flexibility Inductance Capacitance voltage-controlled oscillator (LC-VCO)

The aim of this VCO is to create 3 types of frequencies, which are carrier, modulation, and deviation frequencies, as in equation (1). It is designed as an inductance-capacitance VCO (LC-VCO) structure to minimize the noise and ensure the integrity of the VCO output signal. The basic LC-VCO can produce only the range of the carrier frequency by controlling the varactor's voltage and capacitor bank. **The conventional circuit topology to create the modulation and deviation frequencies is the combination of a phase-locked loop (PLL) and a frequency mixer. This conventional architecture, however, has high complexity that causes large area overhead, high power consumption and long design time.** In this work, a standing-alone LC-VCO is therefore proposed, which can generate all three frequencies (f_C , f_{MOD} , f_{DEV}) with their ranges required by the application.

Fig. 3 shows the schematic of this designed LC-VCO. As previously mentioned, the carrier frequency is created by the basic part in this VCO, whose range is controlled by the DC input ($V_{IN,DC}$) of the varactor C_{DC} and a thermometer code $D_{IN}<14:0>$ of the capacitor bank C_U , which is converted from a 4-bit binary code. Next, in order to generate the f_{MOD} and f_{DEV} , another varactor C_{AC} is added with a sinusoid signal

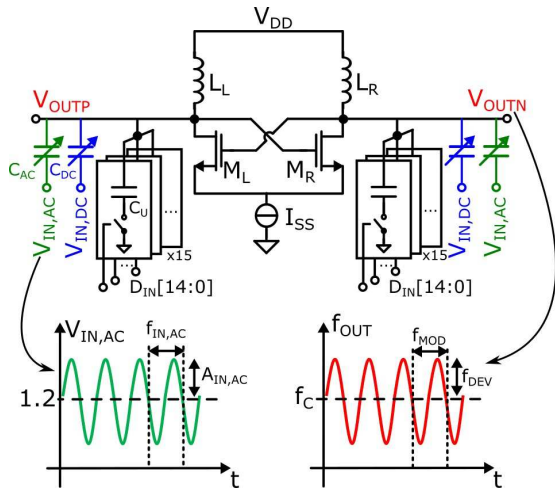


Fig. 3. LC-VCO schematic and frequency tuning.

($V_{IN,AC}$) as its input. As illustrated in Fig. 3, the frequency and amplitude of $V_{IN,AC}$ will be converted to the modulation and deviation frequency, respectively, at the VCO output. By this structure, the VCO output could finally contain the information of all the 3 frequencies.

Regarding the target ranges of the 3 frequencies, the main design constraint is the deviation frequency, especially its lower limit of 1MHz. It could define the maximum frequency fluctuation of the carrier frequency since carrier frequency is the DC component at VCO output (Fig. 3) and its fluctuation could bury the small f_{DEV} values. Therefore, the carrier frequency should perform a fluctuation or frequency noise less than 1 MHz, which is determined by the jitter of the conventional part of VCO.

IV. POST-LAYOUT SIMULATION RESULTS

The chip is designed in a 65nm CMOS technology, and its top-level layout is shown in Fig. 4. The chip has a dimension of 1.72 mm by 1.74 mm. Besides the LDD and LC-VCO a bandgap reference (BGR) is also implemented on-chip to provide a stable voltage and current reference. Excluding the BGR and pads, the core area of the LDD and LC-VCO are 0.31 mm² and 0.48 mm², respectively.

A. Laser Diode Driver

The diode is also modeled according to its characteristics and included in a full system verification [10]. Table 1 presents the post-layout simulated performance. The driving current of LDD is tunable from 88.2 mA to 311.3 mA, and the laser diode power is correspondingly tunable from 21.6 mW to 134.5 mW (the nominal power is 80 mW) in 31 steps. The maximum power noise at the maximum bias current is 92 μ W_{RMS}, which satisfies the noise specification in the application.

Fig. 5 demonstrates the I_F and P_F with or without the designed LDD when the temperature changes from 0°C to

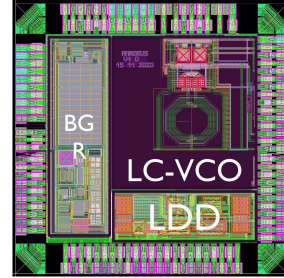


Fig. 4. The chip top-level layout.

Table 1. The simulated LDD features.

Minimum I_F (mA)* / P_F (mW)	88.2	21.6
Maximum I_F (mA)* / P_F (mW)	311.3	134.5
Tuning Step in I_F (mA)* / in P_F (mW)	7.2	3.6
Maximum RMS noise in I_F (μ A)* / in P_F (μ W)	157.5	91.5
I_F setting time (μ s)	170	
Power from 3.3V power supply (mW)**	3.0	

* The I_F -related values are all obtained at the room temperature of 20°C.

** This power excludes the power consumption of the band-gap reference.

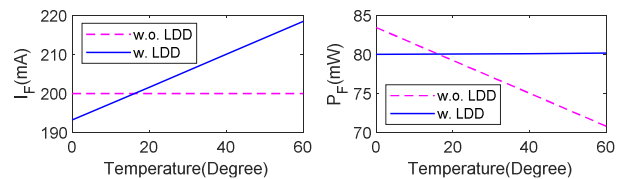


Fig. 5. The I_F and P_F performance with or without (it means to bias the emission diode at a fixed I_F) the LDD when the temperature changes.

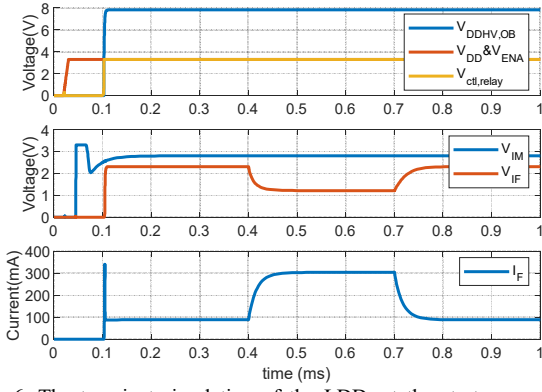


Fig. 6. The transient simulation of the LDD, at the start up and the switching between minimum and maximum of I_F values.

60°C. It indicates that the LDD helps to reduce the power change by 74x from 12.65 mW to 0.17 mW in this temperature range. Importantly, the P_F only experiences a negligible deviation of 0.17 mW at this nominal power condition of 80 mW.

Fig. 6 shows the transient simulation for the LDD during a start-up and the switching between the maximum and minimum I_F (or DAC code). It shows that the high voltage protection works to ensure VDDHV, OB (the supply of diode, as marked in Fig. 2) is high only after the VDD (the supply of LDD) is on. The maximum voltages of V_{IM} and V_{IF} are always below 3.3V, and V_{IM} is successfully stabilized at 2.8 V.

B. LC-VCO

Table 2 summarizes the achieved specifications from the post-layout simulations using grounded and coupling capacitance extracted netlist, which implies that the designed LC-VCO could reach the target ranges of the three created frequencies (carrier, modulation and deviation frequency) with efficient power and area consumption.

Fig. 7 shows a transient simulation of the AC input ($V_{IN,AC}$) and the output of the LC-VCO, as indicated in Fig. 3, when the upper limit values of the f_C , f_{MOD} and f_{DEV} are selected.

Table 2. The simulated LC-VCO performance.

	Specification	Simulation
Carrier frequency	2.37-3.25GHz	2.37-3.25GHz
Modulation frequency	< 100kHz	< 5MHz
Deviation frequency	1MHz – 2MHz	1MHz – 6MHz
Power supply [V]		1.2
Power consumption [mW]		1.8
Area [mm ²]		0.476

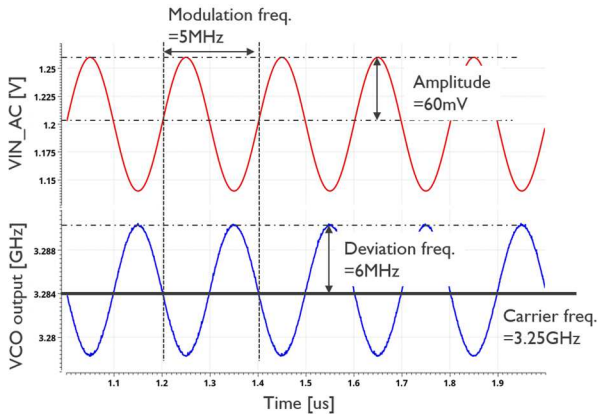


Fig. 7. The AC input $V_{IN,AC}$ and the output of the VCO when the upper limit values of f_C (3.25 GHz), f_{MOD} (5 MHz) and f_{DEV} (6 MHz) are selected.

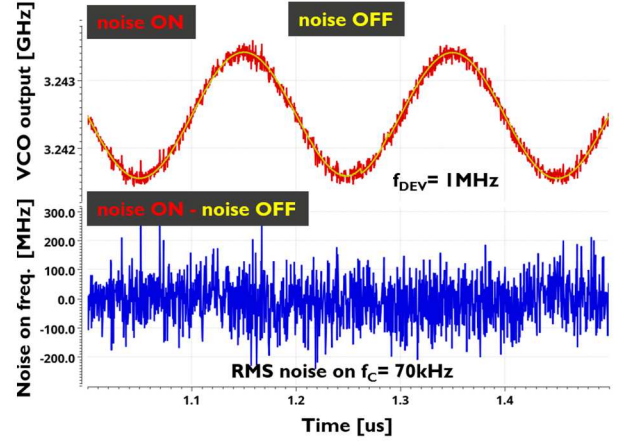


Fig. 8. The f_{DEV} noise simulation at minimum f_{DEV} of 1 MHz when the maximum f_C (3.25 GHz) value is selected.

This confirms that the system could accomplish the reported frequency ranges mentioned in Table 2.

Another important design requirement is that the frequency fluctuation of carrier frequency should be less than the lower limit of deviation frequency, as explained in Section III.B. This is verified by a transient simulation with the noise mode on or off at both the upper and lower limit of the f_C range when the minimum f_{DEV} value (i.e., 1MHz) is selected. Fig. 8 shows the result with the maximum f_C (3.25 GHz), and the f_C RMS noise (or fluctuation) is 70 kHz. The f_C RMS noise with the minimum f_C (2.37 GHz) is also simulated and turns out 39 kHz. As shown, the frequency fluctuation of f_C have been both confirmed far below the minimum f_{DEV} value of 1MHz in the upper and lower limit f_C scenarios.

V. CONCLUSION

This paper presents the miniaturized ASIC solutions of a laser diode driver and a MW source (LC-VCO), in a transportable NV-based quantum magnetic sensor for space exploration. The post-layout simulation result shows that the LDD has a wide driving current tuning range from 88.2 mA to 311.3 mA as well as a temperature-insensitive characteristic with only 0.17mW power deviation at 80mW working power across 60°C temperature range. The LC-VCO could successfully produce the MW frequency range by achieving three tunable parameters: the carrier frequency from 2.37 GHz to 3.25 GHz, the modulation frequency up to 5 MHz and the deviation frequency up to 6 MHz, by a stand-alone design. These two key blocks by the ASIC design now only occupy a compact area of 0.79 mm² and a power consumption of 4.8 mW, which is crucial for a transportable and low-power NV magnetic sensor to be used in the space application.

REFERENCES

- [1] C. L. Degen, "Scanning magnetic field microscope with a diamond single-spin sensor," *Applied Physics Letter*, vol. 92, no. 24, 2008.
- [2] D. Loss and D. P. DiVincenzo, "Quantum computation with quantum dots," *Phys. Rev. A*, vol. 57, no. 1, pp. 120-126, 1998.
- [3] J. F. Barry, et al., "Optical magnetic detection of single-neuron action potentials using quantum defects in diamond," *Proc. Natl. Acad. Sci. U S A*, vol. 113, no. 49, p. 14133–14138, Dec. 2016..

- [4] J. M. Schloss, et al., "Simultaneous Broadband Vector Magnetometry Using Solid-State Spins," *Physics Review Applied*, vol. 10, no. 3, September 2018.
- [5] D. B. Bucher, et al., "Quantum diamond spectrometer for nanoscale NMR and ESR spectroscopy," *Nature Protocols*, vol. 14, no. 9, pp. 2707-47, September 2019. .
- [6] C. Zhang, et al., "Diamond magnetometry and gradiometry towards subpicotesla dc field measurement," *Physical Review Applied*, vol. 15, no. 6, p. 064075, 2021.
- [7] G. Hulot, et al., "NanoMagSat, a 16U Nanosatellite Constellation High-Precision Magnetic Project to Initiate Permanent low-cost Monitoring of the Earth's Magnetic Field and Ionospheric Environment", in EGU21-the EGU General Assembly, 2021.
- [8] J. F. Barry, et al., "Sensitivity optimization for NV-diamond magnetometry," *Reviews of Modern Physics*, vol. 31, no. 92, p. 015004, 2020.
- [9] H. A. R. El-Ella, et al., "Optimized frequency modulation for continuouswave optical magnetic resonance sensing using nitrogen-vacancy ensembles," *Opt. Exp.*, vol. 25, no. 13, pp. 14809–14821, Jun. 2017.
- [10] Green laser diode PLT5 520B in TO56 Package datasheet, Osram Opto Semiconductor, 2015. Available online: https://www.digchip.com/datasheets/parts/datasheet/629/PLT5_520B-pdf.php